TRIUMF	UNIVERSITY OF ALBERTA EDMONTON, ALBERTA	
	Date 1986/11/06	*File No.* TRI-DNA-86-3
Author GM Stinson		*Page* 1 *of* 15
Subject Longitudinal polarization at 230 MeV on beam line 4A		

1. Introduction

An earlier report[1)] presented a study of longitudinal polarization on beam line 1B. One of the possible users of such a beam was the parity experiment. Recently it was suggested that the placement of this experiment on beam line 4A should be investigated in more detail. This requires that the experiment be located downstream of dipole 4AB2 somewhere in the vicinity of the proposed location of the ISOL production target.

Proponents of the parity experiment have requested that the feasibility of such a location be investigated. This report presents the results of such a study for an incident energy of 230 MeV.

2. Design requirements

In their request the experimenters suggested the following requirements.

1. The beam size at the experimental target should be less than 6 mm in diameter.
2. The beam spot should be cylindrically symmetric.
3. The horizontal and vertical beam sizes and divergences are to be independent of momentum.
4. There should be reasonably small beam sizes, preferably waists, in the vicinities of the existing SFU and LD_2 target areas.

This report presents the results of a more detailed study of this problem. It is recalled that coupling of horizontal, vertical, and momentum spaces occurs because of the solenoids and dipoles used to produce longitudinal polarization. This coupling may be partially or completely overcome by the deliberate rotation of phase space elsewhere in the beam line. Rotation of a quadrupole about a beam axis will produce the desired result. Three possible arrangements are discussed in the following sections. Termed the 'coupled', the 'semi-decoupled', and the 'decoupled' cases, they involve increasing numbers of quadrupole rotations.

The *coupled* case is defined to refer to the system that, at the experimental target, produces a beam spot in which the phase-space variables (x, θ, y, ϕ) are coupled to similar variables $(x_0, \theta_0, y_0, \phi_0)$ at the stripper foil but are *not* momentum dependent. This is considered the simplest configuration. The *semi-decoupled* case extends the coupled case by also making the phase-space variable x a function only of x_0 and θ_0 and the variable y a function only of y_0 and ϕ_0. The variables θ and ϕ remain functions of $(x_0, \theta_0, y_0, \phi_0)$. This is a more complicated system that that discussed above. Finally, most complicated is the *decoupled* case. Here, not only are (x, θ, y, ϕ) independent of momentum at the target position but x and θ depend only on x_0 and θ_0 and y and ϕ depend only on y_0 and ϕ_0. This case requires the largest number of quadrupole rotations.

3. Input parameters

Initial phase-space parameters for 230 MeV have been taken from the file TRMF:B4COMBMATRIX. The initial (y_0, ϕ_0) correlation parameter r_{43} was also taken from this file. It is thus assumed that the beam at the stripper foil will have the same characteristics in the new configuration as those that existed in the old. The transfer matrix from the stripper foil to the exit of the combination magnet for an energy of 230 MeV was obtained using a linear interpolation between the calculated values at 220 MeV and 240 MeV. Table 1 lists the input parameters used for the calculations.

4. The coupled case

In order to decouple the (x, θ, y, ϕ) coordinates from momentum it is necessary to to (deliberately) rotate phase space elsewhere in the system. Rotation of quadrupole 4VQ3 is already provided for beam line 4B operation. In addition it was also found necessary to rotate the quadrupole doublet 4AQ6/7 in order to obtain the required results for beam line 4A. The mechanism to rotate 4VQ3 exists; that to accomplish the rotation of 4AQ6/7 is required.

Table 2 lists the beam-transport settings for a beam energy of 230 MeV. The beam profile along the line is shown in the upper portion of figure 1; the experimental target is denoted 4AT3. It is noted that the horizontal divergence of the beam is quite large in both the SFU and LD_2 target areas. Beam profiles in that region are shown on an expanded scale in the lower portion of the figure. Table 3 lists the predicted beam parameters and overall transfer-matrix elements at the polarimeter location upstream of the SFU target, the SFU target location, and the LD_2 target point.

This configuration produces a nominal beam diameter of 4 mm at a point 3.47 m upstream of the wall of the experimental hall. The predicted beam size at the experimental target together with the overall transfer matrix to that point are given in table 4.

Because it was emphasized that cylindrical symmetry of the beam was important, data from the TRANSPORT calculation was used as input for a REVMOC run. The latter program incorporates energy loss and scattering in the stripper foil. Figure 2 shows the REVMOC prediction for the beam spot at the experimental location.

5. The semi-coupled case

In order that further decoupling of the (x, θ) and (y, ϕ) phase spaces be accomplished, it is necessary to allow the rotation of other quadrupoles along the beam line. Assuming that one does not want to modify the beam transport within the vault, there remain only the quadrupole doublet 4AQ4/5 and the triplet 4AQ8/9/10 with which to work. Of these, the latter is more appropriate in that the doublet lies within the vault-wall shielding.

It was found that independent rotation of the individual quadrupoles of the doublet and triplet produced little gain. Consequently, only rotation of the doublet and/or the triplet is considered subsequently.

Rotation of quadrupoles 4VQ3, 4AQ6/7, and 4AQ8/9/10 does not allow complete decoupling of phase spaces. In addition to keeping (x, θ, y, ϕ) independent of momentum at the experimental position, it was decided to decouple x from y_0 and ϕ_0, and y from $(x_0$ and θ_0 there also.

Beam-transport settings to produce this situation are also listed in table 2. The upper portion of figure 3 shows the predicted beam profile along the entire beam line. The lower portion of the figure shows the beam envelope between the SFU and the LD_2 target locations on an enlarged scale, Beam parameters at the intermediate locations are listed in table 5. Predicted beam properties at the experimental target location are given in table 4.

Again, output from the program TRANSPORT was used as input for a REVMOC run. Figure 4 shows the beam spot predicted by REVMOC to be available for the experimenters.

6. The decoupled case

Further decoupling of phase space require the rotation of additional quadrupoles. If one again ignores the remaining vault quadrupoles, only the 4AQ4/5 doublet remains.

The transport settings given in table 2 for the decoupled case produce a beam in which x and θ depend only on x_0 and θ_0, and y and ϕ depend only on y_0 and ϕ_0. This is the same situation one would have were the beam line run in a doubly-achromatic mode except, of course, in this case the beam is also longitudinally polarized. Beam envelopes along the entire beam line are shown in the upper portion of figure 5; those between the SFU and the LD_2 target points are shown on an expanded scale in the lower portion.

Table 6 lists the beam properties and overall transfer-matrix elements at the three intermediate locations. Predicted beam parameters and the overall transfer matrix at the experimental target are listed in table 4.

Figure 6 shows the beam spot predicted at the experimental target by the program REVMOC.

7. Discussion

This report has shown it feasible to produce a longitudinally polarized beam that meets most of the specifications required by the parity experiment. This has been shown true in any of three modes of beam line operation.

All operational modes require that, in addition to quadrupole 4VQ3, the quadrupole doublet AQ6/7 be rotated. Construction of a mechanism to rotate the doublet is not expensive. However, because the experiment is to be performed at a single energy (230 MeV) and because the required rotation of the doublet is small for the coupled and uncoupled cases, it might be more economical to construct a special base to support the doublet at the required angle.

In these calculations no particular requirements were asked at any of the polarimeter, SFU, or LD_2 locations. Rather, attention was paid to the requirements at the longitudinal polarization target position. Consequently, beam sizes at the other locations vary somewhat. It should be recalled that, because of the complete mixing of phase spaces at those points, conventional optical terminology (such as waist and focus) has relatively little meaning.

The beam-spot diameter at the experimental target was nominally 4 mm. Data of table 4 indicate a slightly smaller spot for the decoupled case. Examination of the REVMOC predictions shown in figures 2, 4, and 6, however, indicates that there is not too much to be gained by going beyond the semi-decoupled configuration. In fact, REVMOC predicts that the vertical beam size for the fully decoupled case would be larger than for the other cases. This presumably is due to the large quadrupole rotations required—at least for the solution presented here.

From the data presented here, any of the solutions should satisfy experimental requirements. From a practical point of view, the completely decoupled solution required that quadrupoles 4AQ4/5 be rotated—an extremely difficult operation. This leaves the coupled and semi-decoupled solutions. Of these, the latter should yield a slightly better beam spot. Were the semi-decoupled case chosen, rotation of the 4AQ8/9/10 triplet with a specially designed base is required.

References

1. G. M. Stinson, TRI-DNA-84-4.

Table 1

Input parameters for 230 MeV

Parameter	Value
$\pm x$ (cm)	0.127
$\pm\theta$ (mr)	2.460
$\pm y$ (cm)	0.499
$\pm\phi$ (mr)	0.127
r_{43}	-0.834
R_{11} (cm/cm)	4.6581
R_{12} (cm/mr)	1.4171
R_{16} (cm/%)	4.4852
R_{21} (mr/cm)	5.1107
R_{22} (mr/mr)	1.7523
R_{26} (mr/%)	3.9705
R_{33} (cm/cm)	-1.0275
R_{34} (cm/mr)	0.1567
R_{43} (mr/cm)	-2.1100
R_{44} (mr/mr)	-0.6570

Table 2

Beam transport settings at 230 MeV for longitudinal polarization on beam line 4A

Element	Field (kG)		
	Coupled	Semi-decoupled	Decoupled
4VQ1	2.44926	2.44246	2.44885
4VQ2	−2.87801	−2.90432	−3.13182
Quad rotation (°)	3.44153	3.44271	−0.10185
4VQ3	4.56621	4.65803	5.10805
4VSOL1	2.64274	2.64274	2.64274
4VB1	10.37115	10.37115	10.37115
4VSOL2	−22.14607	−22.14607	−22.14607
Quad rotation (°)	0.0	0.0	26.67184
4AQ4	−4.61145	−4.60609	−3.55490
4AQ5	4.11026	4.11109	4.39266
Quad rotation (°)	1.96982	1.97562	35.70770
4AQ6	3.72648	3.72648	3.44165
4AQ7	−3.25362	−3.25394	−3.18447
4AB2	9.19673	9.19673	9.19673
Quad rotation (°)	0.0	5.80891	68.52520
4AQ8	2.35491	2.37108	0.29098
4AQ9	−2.87869	−2.88936	−2.61291
4AQ10	0.78787	0.78787	2.44165

Table 3

Beam sizes and overall transfer matrices at various locations on beam line 4A
Coupled case at 230 MeV

Parameter	Location		
	Polarimeter	SFU	LD_2
$\pm x$ (cm)	0.190	0.500	0.118
$\pm\theta$ (mr)	11.801	11.801	4.753
$\pm y$ (cm)	0.255	0.318	0.341
$\pm\phi$ (mr)	0.569	1.569	2.855
R_{11} (cm/cm)	0.2602	0.2139	−0.4734
R_{12} (cm/mr)	−0.0607	0.1756	0.0063
R_{13} (cm/cm)	0.1404	−0.4317	−0.0351
R_{14} (cm/mr)	−0.0100	−0.0129	−0.0326
R_{16} (cm/%)	−0.7472	0.6400	0.9814
R_{21} (mr/cm)	−0.8024	−0.8024	−1.8398
R_{22} (mr/mr)	4.0967	4.0967	−1.6714
R_{23} (mr/cm)	−9.9208	−9.9208	4.0585
R_{24} (mr/mr)	−0.0513	−0.0513	0.1163
R_{26} (mr/%)	24.0535	24.0535	−6.4019
R_{31} (cm/cm)	−0.9583	−1.2610	−1.2662
R_{32} (cm/mr)	−0.0064	−0.0025	−0.0161
R_{33} (cm/cm)	0.4248	0.4104	0.0843
R_{34} (cm/mr)	0.4353	0.5716	0.5644
R_{36} (cm/%)	−0.0338	0.0050	0.0000
R_{41} (mr/cm)	−5.2496	−5.2496	11.2710
R_{42} (mr/mr)	0.0644	0.0644	0.0509
R_{43} (mr/cm)	−0.2488	−0.2488	−2.3189
R_{44} (mr/mr)	2.3626	2.3626	−5.1151
R_{26} (mr/%)	0.6727	0.6727	0.0000

Table 4

Beam sizes and overall transfer matrices at the experimental target location

Parameter	Location		
	Coupled	Semi-decoupled	Decoupled
$\pm x$ (cm)	0.192	0.206	0.159
$\pm\theta$ (mr)	1.540	1.577	1.867
$\pm y$ (cm)	0.187	0.195	0.169
$\pm\phi$ (mr)	1.379	1.434	1.447
R_{11} (cm/cm)	1.4394	1.5784	1. 2485
R_{12} (cm/mr)	−0.0127	−0.0195	−0.0030
R_{13} (cm/cm)	0.0908	0.0	0.0
R_{14} (cm/mr)	0.0981	0.0	0.0
R_{16} (cm/%)	0.0	0.0	0.0
R_{21} (mr/cm)	2.2873	2.7010	0.6901
R_{22} (mr/mr)	0.5375	0.5495	0.7353
R_{23} (mr/cm)	−1.2353	−1.3618	0.0
R_{24} (mr/mr)	0.0760	−0.1510	0.0
R_{26} (mr/%)	0.0	0.0	0.0
R_{31} (cm/cm)	0.0460	0.0	0.0
R_{32} (cm/mr)	0.0215	0.0	0.0
R_{33} (cm/cm)	0.3510	0.4062	0.1037
R_{34} (cm/mr)	0.0	0.0451	−0.2379
R_{36} (cm/%)	0.0	0.0050	0.0
R_{41} (mr/cm)	−5.4565	−5.2921	0.0
R_{42} (mr/mr)	−0.0002	0.0653	0.0
R_{43} (mr/cm)	1.5367	1.2915	3.3465
R_{44} (mr/mr)	2.5003	2.6193	2.2509
R_{26} (mr/%)	0.0	0.0	0.0000

Table 5

Beam sizes and overall transfer matrices at various locations on beam line 4A
Semi-decoupled case at 230 MeV

Parameter	Location		
	Polarimeter	SFU	LD_2
$\pm x$ (cm)	0.215	0.520	0.125
$\pm \theta$ (mr)	12.624	12.624	4.950
$\pm y$ (cm)	0.251	0.329	0.366
$\pm \phi$ (mr)	1.776	1.776	3.050
R_{11} (cm/cm)	0.2299	0.2247	−0.4315
R_{12} (cm/mr)	−0.0729	0.1846	0.0201
R_{13} (cm/cm)	0.1425	−0.4278	−0.0315
R_{14} (cm/mr)	−0.0100	−0.0142	−0.0337
R_{16} (cm/%)	−0.7467	0.6405	0.9815
R_{21} (mr/cm)	−0.0909	−0.0909	−1.9585
R_{22} (mr/mr)	4.4656	4.4656	−1.7618
R_{23} (mr/cm)	−9.8898	−9.8898	4.0228
R_{24} (mr/mr)	−0.0729	−0.0729	0.1283
R_{26} (mr/%)	24.0535	24.0535	−6.4023
R_{31} (cm/cm)	−0.9053	−1.1903	−1.1956
R_{32} (cm/mr)	0.0187	0.0310	0.0164
R_{33} (cm/cm)	0.3432	0.3072	−0.0074
R_{34} (cm/mr)	0.4492	0.5895	0.5809
R_{36} (cm/%)	−0.0337	0.0052	0.0001
R_{41} (mr/cm)	−4.9428	−4.9428	10.6487
R_{42} (mr/mr)	0.2128	0.2128	−0.2464
R_{43} (mr/cm)	−0.6236	−0.6236	−1.4381
R_{44} (mr/mr)	2.4330	2.4330	−5.2751
R_{26} (mr/%)	0.6749	0.6749	−0.0009

Table 6

Beam sizes and overall transfer matrices at various locations on beam line 4A
Decoupled case at 230 MeV

Parameter	Location		
	Polarimeter	SFU	LD_2
$\pm x$ (cm)	0.406	0.930	0.572
$\pm\theta$ (mr)	9.245	9.245	5.941
$\pm y$ (cm)	0.291	0.360	0.340
$\pm\phi$ (mr)	3.447	3.447	2.942
R_{11} (cm/cm)	−0.0514	−0.5109	−0.7042
R_{12} (cm/mr)	0.1515	0.2572	0.2016
R_{13} (cm/cm)	−0.2972	−0.3794	−0.4961
R_{14} (cm/mr)	−0.1644	−0.1877	−0.3344
R_{16} (cm/%)	0.2846	1.1316	0.9815
R_{21} (mr/cm)	−7.9693	−7.9693	2.8604
R_{22} (mr/mr)	3.5667	3.5667	−2.2712
R_{23} (mr/cm)	−1.4247	−1.4247	2.7286
R_{24} (mr/mr)	−0.4042	−0.4042	2.0657
R_{26} (mr/%)	14.6861	14.6861	−6.4022
R_{31} (cm/cm)	−0.0307	−0.2336	−0.0800
R_{32} (cm/mr)	−0.0188	0.0527	−0.1199
R_{33} (cm/cm)	0.6626	0.7313	0.1367
R_{34} (cm/mr)	0.3872	0.5247	0.3136
R_{36} (cm/%)	0.1136	0.5132	0.0000
R_{41} (mr/cm)	−3.5190	−3.5190	−0.4705
R_{42} (mr/mr)	1.2401	1.2401	0.5801
R_{43} (mr/cm)	1.1905	1.1905	−5.4737
R_{44} (mr/mr)	2.3855	2.3855	−4.3806
R_{26} (mr/%)	6.9305	6.9305	0.0000

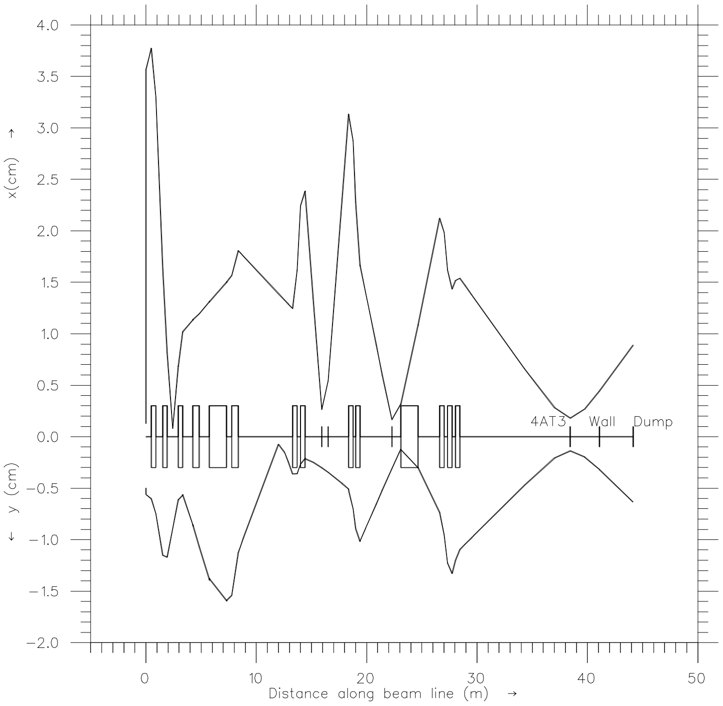

Fig. 1a. Beam envelope on beam line 4A – Coupled case.

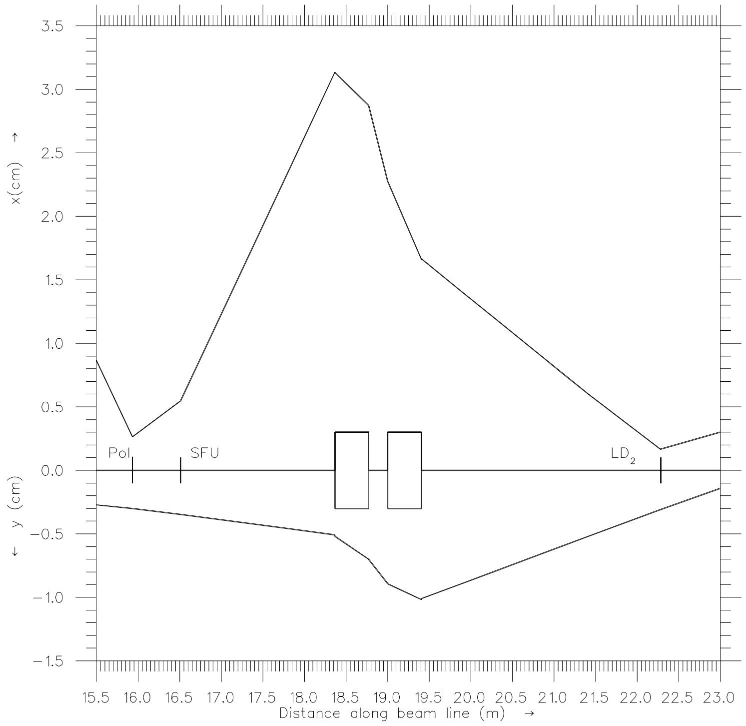

Fig. 1b. Beam envelope between the SFU and LD_2 targets – Coupled case.

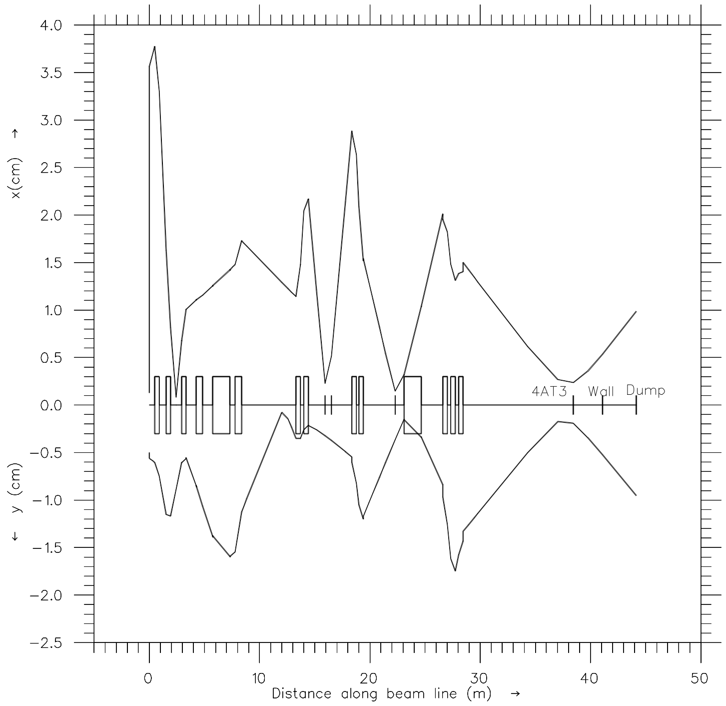

Fig. 3a. Beam envelope on beam line 4A – Semi-coupled case.

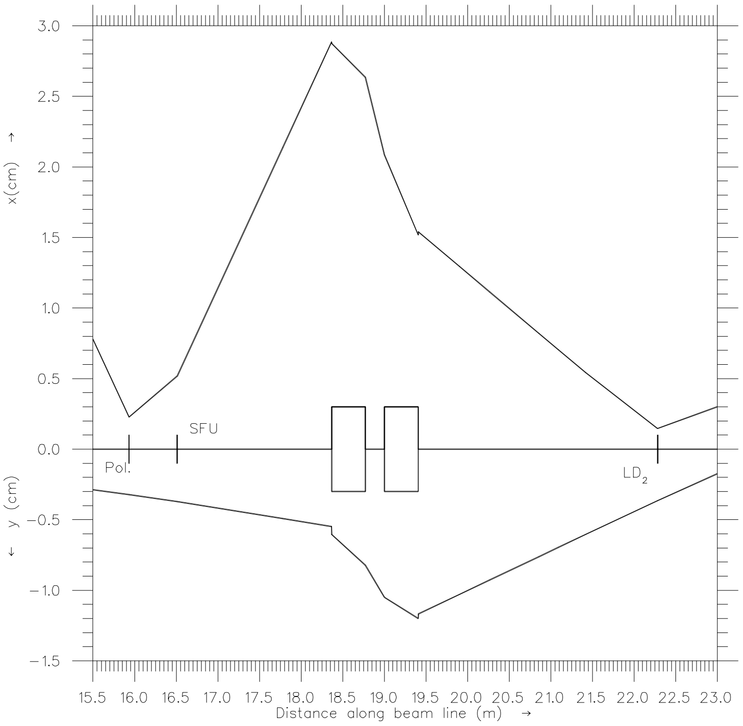

Fig. 3b. Beam envelope between the SFU and LD_2 targets – Semi-coupled case.

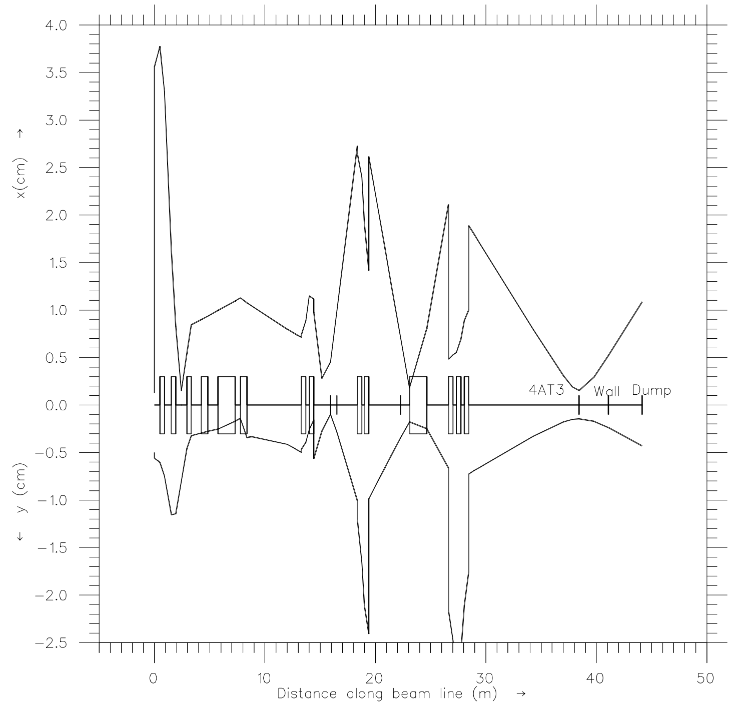

Fig. 5a. Beam envelope on beam line 4A –Decoupled case.

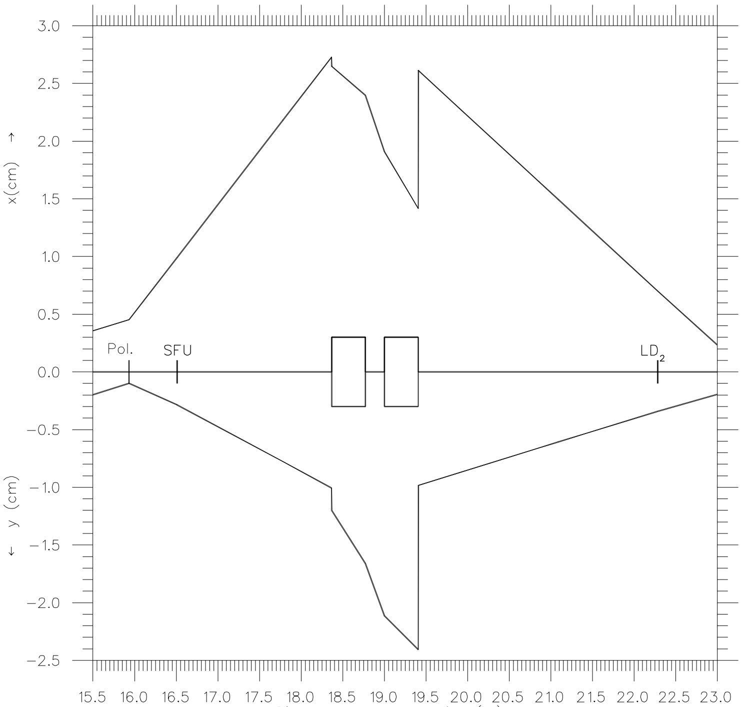

Fig. 5b. Beam envelope between the SFU and LD_2 targets –Decoupled case.